THE JOURNAL OF PHYSICAL CHEMISTRY C
A JOURNAL OF THE AMERICAN CHEMICAL SOCIETY

pubs.acs.org/JPCC

Article

A Fresh Look at a Well-Known Solid: Structure, Vibrational Spectra, and Formation Energy of $NaNH_2$

Published as part of The Journal of Physical Chemistry virtual special issue "Early-Career and Emerging Researchers in Physical Chemistry Volume 2".

Laura Bonometti, Florian Kraus, Tim Graubner, Antti J. Karttunen, Bartolomeo Civalleri, Lorenzo Donà, and Lorenzo Maschio*

Cite This: *J. Phys. Chem. C* 2023, 127, 12287−12294

Read Online

ACCESS | Metrics & More | Article Recommendations | Supporting Information

ABSTRACT: Sodium amide ($NaNH_2$) in its α form is a common compound that has recently seen renewed interest, mainly for its potential use as a solid-state hydrogen storage material. In this work, we present a synergic theoretical and experimental characterization of the compound, including novel measured and simulated vibrational spectra (IR and Raman) and X-ray diffraction patterns. We put forward the hypothesis of a low-temperature symmetry breaking of the structure to space group $C2/c$, while space group *Fddd* is commonly reported in the literature and experimentally found down to 80 K. Additionally, we report a theoretical estimate of the heat of formation of sodium amide from ammonia to be equal to −12.2 kcal/mol at ambient conditions.

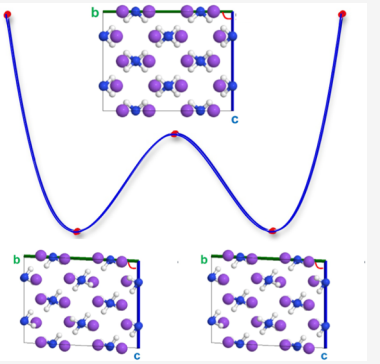

INTRODUCTION

Solutions of alkali and alkaline earth metals in liquid ammonia have drawn the attention of the scientific community since the beginning of the last century for their use in strictly chemical or electrochemical processes.[1−6] The typical reaction that takes place leads to the formation of amides MNH_2 (M = alkali metal), and they can be schematized as

$$M_{(s)} + NH_{3(l)} \rightarrow MNH_{2(s)} + \frac{1}{2}H_{2(g)} \quad (1)$$

This reaction has been characterized from different points of view, from kinetics[7] to the equilibrium constant,[8] from the catalysis[7,9] to electrical conductivity,[1] and so forth. $NaNH_2$ can also act as an intermediate in the decomposition of ammonia to nitrogen and hydrogen.[10]

Recently, amides of alkali metals together with lightweight metal hydrides have drawn attention as solid-state hydrogen storage materials.[11−17] The most extensively studied one is probably lithium amide ($LiNH_2$), which is characterized by great storage capacities (8.7 wt % of hydrogen content).[15−17] Among these materials, $NaNH_2$ is of considerable interest because of its role in the dehydrogenation of other light metal hydride systems, by forming composite hydrogen storage materials, as in $NaNH_2$−$LiBH_4$ and others.[18−21] Moreover, sodium is not such a critical raw material as lithium.

Sodium amide has been characterized from different points of view: structural and electronic properties[22−27] have been investigated together with vibrational properties,[23,28,29] both at ambient conditions and at high pressures. Nonetheless, the number of theoretical studies of solid $NaNH_2$ seems not to be very large to date.[23,25,30]

In this paper we intend to partly fill this gap, by (i) studying its structural stability and actually unveiling a possible low-temperature symmetry breaking; (ii) simulating IR and Raman spectra, with subsequent vibrational modes assignment; and (iii) simulating powder XRD patterns. All computed properties are complemented by and compared with new, original experimental data. Furthermore, we also evaluate computationally the heat of reaction of eq 1 at ambient conditions and at the athermal limit.

The paper is organized as follows: in the next section, experimental and computational details are reported, followed by the results of our work, unveiling a symmetry breaking from the *Fddd* to a $C2/c$ structure; powder X-ray diffraction patterns, heat of reaction calculations, as well as vibrational spectra (IR and Raman) are discussed; in the last section, final conclusions of our work are summarized.

Received: March 28, 2023
Revised: May 24, 2023
Published: June 13, 2023

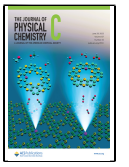

METHODS

Computational Details. We used a development version of the CRYSTAL23 code[31] for all the calculations, which adopts atom-centered Gaussian-type functions, along with a PBE0[32] hybrid exchange-correlation functional. van der Waals dispersion interactions were accounted for through the empirical DFT-D4 method,[33−35] which improves upon the D3 dispersion correction scheme especially for ionic systems. The adopted basis sets are pob-TZVP-rev2[36] for N and H and pob-TZVP for Na.[37] The integration over the Brillouin zone in the reciprocal space was performed using a 8 × 8 × 8 Monkhorst−Pack grid for $NaNH_2$, a 12 × 12 × 12 grid for Na, considering a 2 × 2 × 2 supercell, and a 6 × 6 × 6 grid for NH_3. The thresholds that control the five truncation criteria (T_i) of the Coulomb and exchange infinite lattice series have been set to 7 (T_1−T_4) and 25 (T_5). The threshold for convergence on total energy has been set to 10.

The vibrational mode frequencies are evaluated according to the harmonic approximation, the Hessian is evaluated as the numerical derivative of first-order analytical gradients, and intensities are computed through a coupled-perturbed scheme.[38]

Experimental Details. From the experimental side, all work was carried out trying to exclude moisture and air in an atmosphere of dried and purified argon (5.0, Praxair) using high-vacuum glass lines and a glovebox (MBraun). Liquid ammonia was dried by storage over Na. The glass vessels were flame-dried under fine vacuum several times before utilization.

Synthesis. Na (Acros, >99.5%) was freed from any crusts under hexanes and placed into a flame-dried Schlenk vessel under Ar. After pumping off any residual hexanes, the Na was molten in vacuum using a Bunsen burner and slowly poured into an attached glass ampule and flame-sealed. Any hydroxides or oxides present stuck to the glass surface of the Schlenk vessel, and pure Na flowed into the ampule. A flame-dried borosilicate glass ampule with 8 mm inner diameter was charged in the glovebox with Na metal (12 mg, 0.5 mmol); the ampule was closed using a glass valve, taken out of the glovebox, and attached to a Schlenk line for the work with anhydrous NH_3. In an Ar counter stream, a trace amount of rust was added to catalyze the reaction. The ampule was evacuated and cooled to −78 °C using dry ice/isopropanol; ca. 2 mL of NH_3 was distilled into it, and the Na dissolved first with bronze and then with blue color. The ampule was then cooled to liquid N_2 temperature and flame-sealed under vacuum. The sealed-off tube was stored for 6 h at room temperature during which the solution became colorless and colorless $NaNH_2$ precipitated in quantitative yield. To grow crystals large enough for the diffraction experiment, the flame-sealed ampule was placed into a heating block at 40 °C for 5 days. The ampule was cooled to liquid nitrogen temperature and cut open under Ar, and the residual NH_3 evaporated at room temperature and then under vacuum. $NaNH_2$ was obtained as a white powder in quantitative yield.

Powder X-ray Diffraction. The sample was filled into a predried borosilicate glass capillary with a diameter of 0.3 mm. The powder X-ray pattern was recorded with a StadiMP diffractometer (Stoe & Cie) in the Debye−Scherrer geometry. The diffractometer was operated with Cu−Kα1 radiation (1.5406 Å, germanium monochromator) and equipped with a MYTHEN 1K detector. The diffraction pattern was indexed using the WinXPOW suite.[39]

IR and Raman Vibrational Spectroscopy. Infrared spectra were measured on a Bruker Alpha Platinum FT-IR spectrometer using the ATR Diamond module with a resolution of 4 cm^{-1}. The spectrometer was located inside a glovebox under argon (5.0, Praxair) atmosphere. For data collection, the OPUS 7.2 software was used.[40]

The Raman spectra were measured at room temperature with a Monovista CRS+ confocal Raman microscope (Spectroscopy & Imaging GmbH) using a solid-state laser (488/532/633 nm) and a 300 grooves/mm (low-resolution mode, fwhm: <5.50 cm^{-1} (488 nm)/<4.62 cm^{-1} (532 nm)/<3.25 cm^{-1} (633 nm)) grating.[41] The sample was measured inside a borosilicate glass ampule.

X-ray Structure Determination at 80 K. Single crystals were selected under a predried argon stream in perfluorinated polyether (Fomblin YR 1800, Solvay Solexis) and mounted using the MiTeGen MicroLoop system at ambient temperature. X-ray diffraction data was collected using the monochromated Cu−Kα (λ = 1.54186 Å) radiation of a Stoe StadiVari diffractometer equipped with a Xenocs Microfocus Source and a Dectris Pilatus 300 K detector. Evaluation, integration, and reduction of the diffraction data were carried out using the X-AREA software suite.[42] Multiscan absorption correction was applied with the LANA module of the X-AREA software suite. The structure was solved with dual-space methods (SHELXT-2018/2) and refined against F^2 (SHELXL-2019/2) using the SHELXLE software package.[43−45] All atoms were located by difference Fourier synthesis and non-hydrogen atoms refined anisotropically. Hydrogen atoms were located from difference Fourier syntheses and freely refined isotropically. CCDC 2250356 contains the supplementary crystallographic data for this paper. This data can be obtained free of charge from The Cambridge Crystallographic Data Centre.

RESULTS AND DISCUSSION

Structure and Stability. *Hypothesis for a Symmetry Breaking in the $NaNH_2$ Structure.* Literature reports that the thermodynamically most stable polymorph of $NaNH_2$ at ambient conditions is the orthorhombic α structure (space group *Fddd*, 70).[14,22,23] After a first geometry optimization in that symmetry, however, we found one imaginary frequency (about 112*i* cm^{-1}, B_{2g} symmetry), indicating this structure is not a true local minimum.

We show in Figure 1 the computed potential energy surface along this normal mode, which actually shows that a lower-energy structure follows from symmetry breaking—the

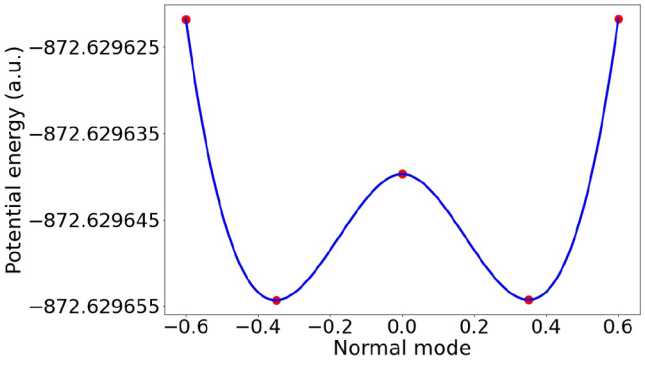

Figure 1. Potential energy (a.u.) along the first normal mode.

https://doi.org/10.1021/acs.jpcc.3c02059
J. Phys. Chem. C 2023, 127, 12287−12294

Table 1. Cell Parameters (Å), α Angle, and Volume (V) (Å^3) of Experimental Lattice Parameters[22] Obtained from Powder Diffraction at Room Temperature, Experimental Geometry Determined at 80 K from Single Crystal X-ray Diffraction, and Optimized Geometries[a]

α-$NaNH_2$	a	b	c	α	V
exp.(293 K)[22]	8.949(6)	10.456(5)	8.061(4)	90°	754.27(7)
exp.(80 K)	8.959(6)	10.368(9)	7.978(6)	90°	741.02(10)
calc. *Fddd*	8.935 (−0.3%)	10.014 (−3.4%)	7.763 (−2.7%)	90° (0%)	694.60 (−6.3%)
calc. *C*2/*c*	8.872 (−1.0%)	10.093 (−2.7%)	7.787 (−2.4%)	92.41° (+2.7%)	696.50 (−6.0%)

[a]In parentheses, standard uncertainties of experimental values and deviations of the calculated results from experimental geometry at 80 K are shown.

corresponding subgroup is monoclinic, *C*2/*c*. In Figure 1, the red dots are the results of our calculations, while the blue curve is the result of cubic spline interpolation of our data.

We reoptimized the structure from the observed minimum, and detailed information is found in Table 1.

Such symmetry breaking is not uncommon and is similar to what we recently observed in a different system, namely Li_6PS_5Cl.[46] Clearly, the energy barrier between the optimized structures in *Fddd* and *C*2/*c* space groups is very small (only about 0.02 eV), and thus, already at this stage, we do not expect such symmetry breaking to be measurable at room temperature conditions.

Figure 2 shows that the structural difference between the optimized geometries is not very large, the most notable

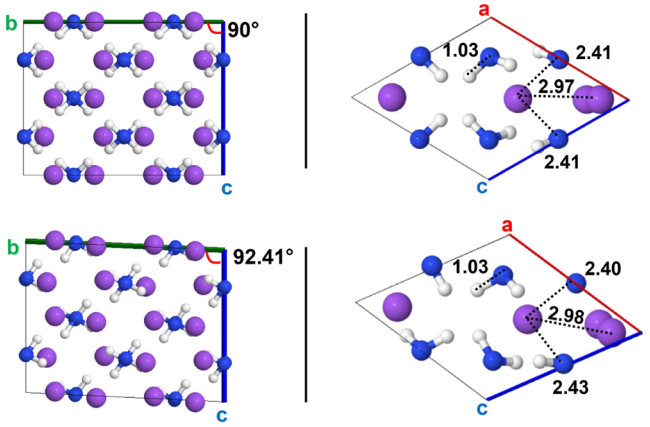

Figure 2. On the left, representations of the crystal structures and conventional cells (top: structure in the *Fddd* space group; bottom: structure in the *C*2/*c* space group) with highlighted α angle; on the right, representation of the primitive cells with highlighted bond (Å). Color code: Na purple, N blue, H white.

features being a slight change in the alpha angle, a variation in the a and b lattice parameters, and a change in Na−N distances.

As expected, the change in the computed electronic structure is also not too relevant: the band gap is 4.29 eV for $NaNH_2$ in space group *C*2/*c* and 4.27 eV in space group *Fddd*. Such values—computed with hybrid functionals—are larger than those obtained from LDA calculations in previous works.[23,30]

Compared with the experiments, our optimized cell is about 6% smaller in volume. Considering that our calculations are carried out at the athermal limit and the delicate balance of the whole computational setup, we deem such a result more than satisfactory.

X-ray Diffraction Pattern. In order to investigate further the *Fddd* vs *C*2/*c* puzzle of solid $NaNH_2$, we carried out single crystal X-ray diffraction at 80 K of sodium amide single crystals. A splitting of the reflections at high angles would potentially indicate a lowering to monoclinic symmetry. The structure resulted, however, to be still orthorhombic *Fddd*, and no splitting of reflections was observed. Considering the low energy difference between the two structures and that all atoms show very strong thermal vibrations,[22] it is likely that the phase transition occurs at lower temperatures. For this reason, additional investigations could be performed, such as a measurement of heat capacitites down to 2 K and neutron diffraction patterns, which we leave for future work.

We computed the powder X-ray diffraction (PXRD) pattern for $NaNH_2$ in both *Fddd* and *C*2/*c* space groups, considering an incident wavelength equal to 1.5406 Å, correspondent to the Cu−Kα1 line. In Table 2 and Figure 3 we compare such a computed pattern with our experimental one and experimental data from the literature.[24]

Table 2. Comparison of Powder X-ray Diffraction Pattern's Peaks among Experimental and Calculated Results[a]

	$2\theta^\circ$		
hkl	exp.[24]	exp.	calc. *Fddd*
111	17	17.047	17.44 (+2.3%)
220	26	26.194	26.50 (+1.2%)
022	27	27.929	28.97 (+3.7%)
131	29	29.631	30.52 (+3.0%)
311	33	33.121	33.23 (+0.3%)
113	36	35.908	37.22 (+3.7%)
400	40	40.279	40.10 (−0.4%)
331	41	41.351	41.93 (+1.4%)
133	43.5	43.687	45.27 (+3.6%)
004	45	44.944	46.79 (+4.1%)
422	49	49.727	50.22 (+1.0%)
224	53	52.802	54.58 (+3.4%)
153	57	56.636	58.75 (+3.7%)
260	57	56.636	58.35 (+3.0%)
404	62	61.920	63.28 (+2.2%)

[a]Experimental results are obtained at room temperature, while the calculated ones are referred to the optimized structure at the athermal limit. In parentheses, the deviations of calculated values from observed ones are given.

The *Fddd*-$NaNH_2$ structure type pattern compares better to the experimental one, confirming the hypothesis that the monoclinic structure is just the low-temperature polymorph of sodium amide. Changing the symmetry, peak indexing is changing, and a splitting of reflections occurs. For this reason, a direct comparison of peak assignment for the calculated

https://doi.org/10.1021/acs.jpcc.3c02059
J. Phys. Chem. C 2023, 127, 12287−12294

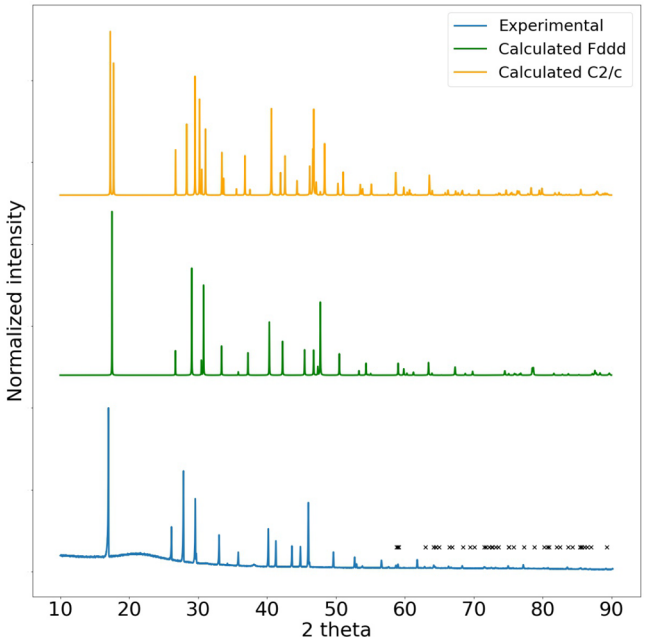

Figure 3. Experimental and calculated XRD patterns comparison. Experimental results are obtained at room temperature, while the calculated ones are referred to the optimized structure at the athermal limit. Peaks marked with the x symbol were not assigned.

pattern of structure in the $C2/c$ space group and experimental results would not be consistent and is not presented. The detailed peak assignment can be found in the Supporting Information.

The maximum deviation from the experimental 2θ angle is about 4.5% for $NaNH_2$ in the *Fddd* space group. Differences in the calculated and experimental pattern of structure in the *Fddd* space group can be noticed. It is expected since the experimental pattern was recorded at room temperature whereas the calculated ones are referred to athermal limit simulated structures. Therefore, reflection positions will be different due to the temperature dependence of the lattice parameters, leading to some discrepancy. Moreover, the intensities could differ because of the thermal motion of the atoms.

At higher diffraction angles the comparison becomes difficult due to the low intensity of the experimental peaks—because of X-ray atomic form factors and interactions of X-rays with electrons of the atoms. For this reason, in Table 2 we reported just the comparison of the most intense peaks. The reflections we could not assign are marked with an x symbol in the pattern in Figure 3. Anyway, these peaks are surely related to $NaNH_2$ because reflections of alien phases would show up at lower diffraction angles, additionally.

Prediction of the Heat of Formation from Ammonia. In order to evaluate the formation energy of $NaNH_2$ (eq 1), we first performed a full geometry optimization for all the other structures involved, namely metallic Na, solid NH_3, and lastly the H_2 molecule. The optimized cell parameter for Na is 4.027 Å (space group $Im\bar{3}m$ (229), lattice parameter a = 4.235 Å[47]), while for NH_3 it is 4.949 Å (space group $P2_13$ (198), lattice parameter a = 5.048 Å[48,49]). As expected, the band structure for Na shows metallic character, and the band gap of solid ammonia is equal to 7.02 eV. A reduction (about −5%) in the lattice parameter of sodium with respect to values reported in literature is obtained.[47] It is well-known, in fact, that the choice of the basis set for the treatment of metallic systems is crucial, and very diffuse functions are needed to correctly reproduce the density characterizing them. However, in order to obtain comparable results with the other studied compounds, a coherent level of theory was necessary, leading to the choice of the pob-TZVP basis set for Na, which Peintinger et al.[37] indicated as suitable for the study of metallic sodium too, without the addition of diffuse valence functions.

We computed the heat of the reaction as

$$\Delta H^\circ = \sum_p \nu_p \Delta H_p - \sum_r \nu_r \Delta H_r \quad (2)$$

where p is the index for the products and r is the index for the reagents.

The thermodynamic function for ambient conditions was obtained from the frequency calculations (using a 2 × 2 × 2 supercell in the case of metallic Na). Results are reported for all the species involved in the reaction in Table 3.

Table 3. Thermodynamic Functions (a.u./cell for Solids and a.u. for H_2) at 298.15 K and 0.101325 MPa of the Na 2 × 2 × 2 Supercell, NH_3, *Fddd*- and $C2/c$−$NaNH_2$, and H_2[a]

	EL	E0	ET	PV
Na supercell	−1297.667964	0.005261	0.015110	0.000006
NH_3	−226.081078	0.152115	0.008553	0.000003
H_2	−1.166063	0.010125	0.002360	0.000944
Fddd-$NaNH_2$	−872.629640	0.098224	0.014555	0.000004
$C2/c$-$NaNH_2$	−872.630207	0.099387		
	H(298.15 K)		H(0 K)	
Na supercell	−1297.647586		−1297.662702	
NH_3	−225.920407		−225.928963	
H_2	−1.152633		−1.155938	
Fddd-$NaNH_2$	−872.516857			
$C2/c$-$NaNH_2$			872.530820	

[a]EL = electronic energy, E0 = zero-point energy, ET = thermal contribution to the vibrational energy, PV = pressure by volume, H(298.15 K) = EL + E0 + ET + PV; H(0 K) = EL + E0. For $C2/c$-$NaNH_2$ just EL, E0, and H at the athermal limit are reported; for *Fddd*-$NaNH_2$ EL, E0, ET, PV, and H at 298.15 K are reported.

Our estimate for the heat of reaction at 298.15 K is −12.2 kcal/mol (−51.1 kj/mol) for $NaNH_2$ in space group *Fddd*, since it is the stable polymorph at ambient conditions, which is in very good agreement with previously reported experimental values of −12.3[50] and −11.7 kcal/mol.[51] At the athermal limit, our ΔH^0 estimate is −12.9 kcal/mol (−54.1 kj/mol) for $NaNH_2$ in space group $C2/c$, since it is supposed to be the equilibrium structure at low temperature. By increasing the supercell size, such results change only marginally (0.35 kcal/mol).

Vibrational Spectra. *Infrared Spectrum.* We simulated the IR spectrum of $NaNH_2$ in both *Fddd* and $C2/c$ space groups, which we report in Figure 4 and Table 4. The experimental IR spectrum was recorded at ambient temperature, while simulated IR is at the athermal limit. At a first glance it is evident that the computed spectra are both in general agreement with our experimental one which, in turn, is fully coherent with the available literature data.[28,29] The most notable discrepancy is found in the range 800−1500 cm^{-1} where some unpredicted features appear in the experimental spectrum. These peaks are not visible even in other experimental IR spectra reported in the literature, and we

https://doi.org/10.1021/acs.jpcc.3c02059
J. Phys. Chem. C 2023, 127, 12287−12294

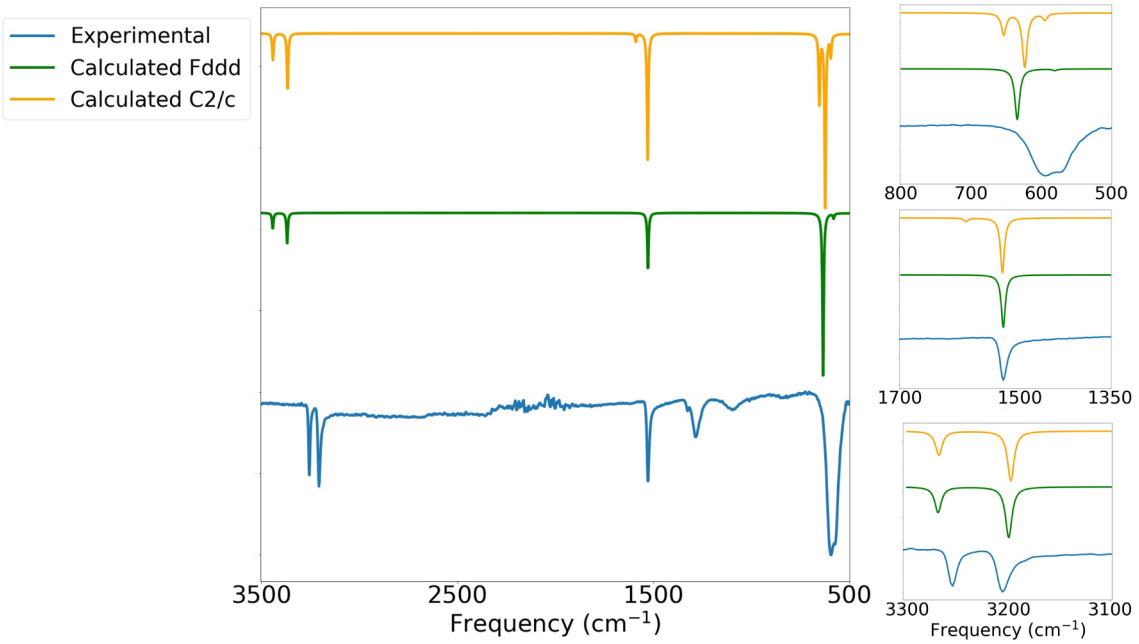

Figure 4. On the left, experimental (room temperature) and calculated (athermal limit) IR spectra comparison of $NaNH_2$ for the different optimized geometries; on the right, zoomed-in IR spectra zones (in order from top to bottom: 500−800, 1350−1700, and 3100−3300 cm^{-1} (scaled by a factor of 0.95)). The calculated spectra are convoluted with a full width at half-maximum of 8 cm^{-1}.

Table 4. Experimental (Room Temperature) and Calculated (Athermal Limit) IR Frequencies (cm^{-1}) Comparison of $NaNH_2$ for the Different Geometries[a]

exp.[28]	exp.	calc. *Fddd*	calc. *C2/c*
		580	595
609	591		623
		634	653
1530	1528	1528	1529
3212	3208	3368 (3200)	3366 (3198)
3259	3257	3442 (3270)	3441 (3269)

[a]In parentheses, scaled values of frequencies (scale factor = 0.95) can be found.

were not able to identify their origin. Overall, the simulated IR spectra for the orthorhombic and monoclinic structures do not show significant differences. Let us look more in detail at the specific frequency ranges.

The band reported at the 609 cm^{-1} wavenumber in the work of Liu and Song[28] and corresponding to the 591 cm^{-1} wavenumber in our experimental spectrum is a very broad one, and it may be related to the convolution of three or more bands since the shape is not as well-defined as the other ones. In all our simulations, we notice a rigid shift in the group of frequencies, as a direct consequence of the underestimation of the cell volume reported in the previous section and harmonic approximation, reflected on these collective vibrational modes. In the IR spectrum simulated for the structure with *C2/c* symmetry, the appearance of three bands can be observed, while the *Fddd* spectrum reports in this region an intense band at 634 cm^{-1} and a weak one at 580 cm^{-1}. However, even if the broadening of the experimental band can be related to the convolution of more bands, its origin could possibly be of a different nature.

In the other regions we see no decisive feature in the spectra for the different structures, all in good agreement with the experiment. An extra band with weak intensity is estimated to be around 1590 cm^{-1} in the simulated spectrum for the *C2/c* space group, and it is related to bending of the N−H bond. After the usual rescaling of the frequencies due to anharmonicity (we adopted here a factor of 0.95), also the high-frequency H-stretching modes compare well.

Raman Spectrum. We computed powder (direction-averaged) Raman spectra for the different structures of $NaNH_2$, using the same algorithm as described above for band positions and analytical evaluation of intensities.[52] We took also into account the experimental conditions (temperature and laser wavelength) to calculate Raman intensities. The experimental Raman spectrum was measured using three different lasers working at 488, 532, and 633 nm. For comparison with the calculated data, we considered the 488 nm one.

In Figure 5, a comparison among calculated and experimental spectra is presented, while in Table 5 the frequencies of the most intense bands are reported for a comparison among data from the literature, our experimental results, and calculated ones. The experimental Raman spectrum was recorded at room temperature, and the simulated spectrum was obtained by setting the temperature equal to 298 K and the incoming laser wavelength equal to 488 nm.

In the low-frequency region of the Raman spectrum, the number of bands in the calculated spectra is higher than that of the experimental one. It is worth remembering here that the computed intensity is interpreted as the band height, and a uniform broadening is applied, while this quantity is more properly to be interpreted as the band area. It is clear here that the experimental bands—especially those in the 400−600 cm^{-1} region—all have different broadening, much larger than the reported ones, and hence they may largely overlap with each other. For instance, the experimental bands at 470 and 533 cm^{-1} may well be the convolution of two of the four bands which are individuated in the calculated spectra for *Fddd* and

https://doi.org/10.1021/acs.jpcc.3c02059
J. Phys. Chem. C 2023, 127, 12287−12294

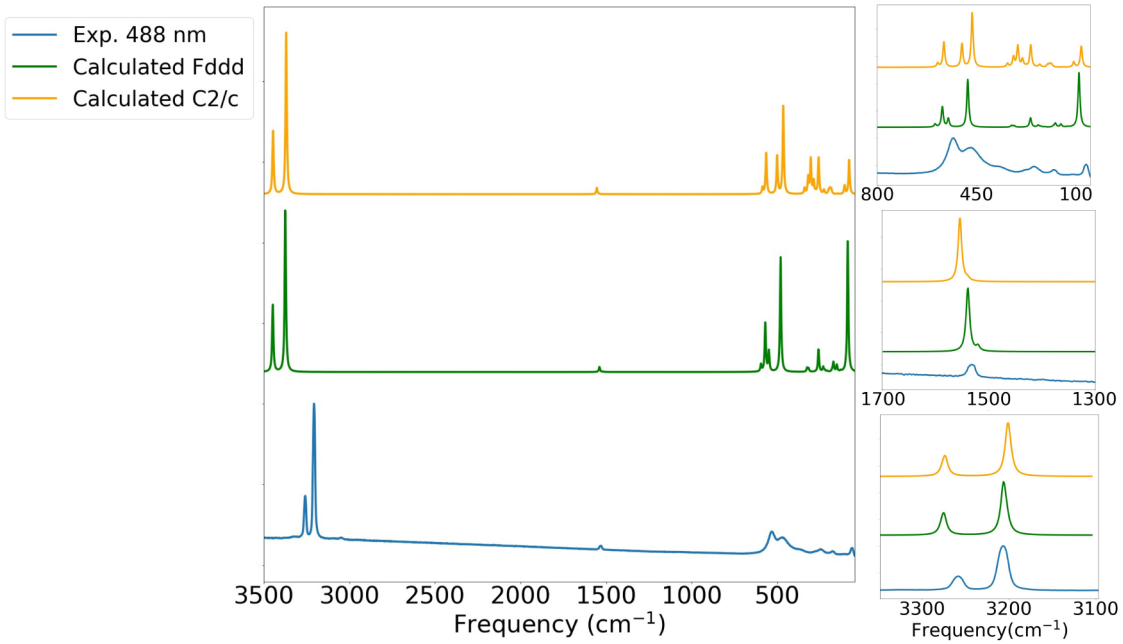

Figure 5. On the left, room temperature experimental and calculated Raman spectra comparison of $NaNH_2$ for the different optimized geometries; on the right, zoomed-in Raman spectra zones (in order from top to bottom: 50−800, 1300−1700, and 3100−3350 cm^{-1} (scaled by a factor of 0.95)). The calculated spectra are convoluted with a full width at half-maximum of 8 cm^{-1}.

Table 5. Experimental (Room Temperature) and Calculated (298 K) Raman Frequencies (cm^{-1}) Comparison of $NaNH_2$ for the Different Geometries[a]

exp.[28]	exp.[53]	exp.	calc. *Fddd*	calc. *C2/c*
115		62	89	81
				108
177		177	172	185
			152	192
				200
251		247	259	259
			232	288
	349	380	326	305
			317	320
464	468	470	481	465
			506	501
535	522	533	549	565
			570	587
1536	1531	1532	1539	1554
3210	3218	3207	3375 (3206)	3370 (3202)
3261	3267	3258	3447 (3275)	3445 (3273)

[a]In parentheses, scaled values of frequencies (scale factor = 0.95) can be found.

C2/c structures, which are reported in Table 5. The same can be observed for experimental bands at 177, 247, and 380 cm^{-1}. A blue shift of bands can be noticed as observed in the IR, but no crucial differences can be individuated between the simulated Raman spectra of orthorhombic and monoclinic structures.

In the region around 1500 cm^{-1}, only one bands appears, corresponding to the symmetric bending of the N−H bond. It is possible to find a better agreement between the experimental frequency and the calculated one for the *Fddd* structure, as expected since the orthorhombic polymorph is the most stable one at room temperature. However, an extra shoulder band appears in the *Fddd* system.

The calculated frequencies of the bands in the high-wavenumber region have been once more downscaled to empirically account for missed anharmonic effects (scale factor = 0.95). However, we found no valuable information in the analysis of these particular bands.

Furthermore, we calculated the anisotropic displacement parameters (ADPs) for all the structures. ADP is a 3 × 3 tensor associated with each atom of the unit cell. Diagonalizing the resulting tensors, we obtained three positive eigenvalues for each irreducible atom of the cell which define the length of the principal axes of the ellipsoids. The ellipsoids define the surfaces of constant probability of atomic displacement. In Figures 6 and 7 we show the calculated ADPs for structures in the *Fddd* and *C2/c* space groups, respectively. As can be seen, the ADPs of all atoms, especially for hydrogens, of the structure in the *Fddd* space group are larger than those of the monoclinic structure. This observation seems to be in agreement with that reported by Nagib et al.[22] We observed the same behavior by considering $NaND_2$ in both *Fddd* and

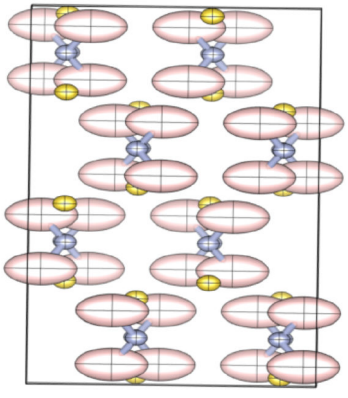

Figure 6. *Fddd*-$NaNH_2$ anisotropic displacement ellipsoids. Color code: Na yellow, N blue, and H pink.

https://doi.org/10.1021/acs.jpcc.3c02059
J. Phys. Chem. C 2023, 127, 12287−12294

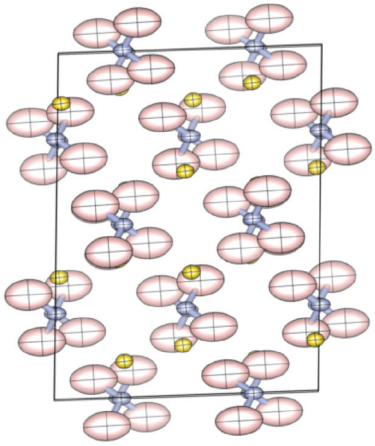

Figure 7. C2/*c*-$NaNH_2$ anisotropic displacement ellipsoids. Color code: Na yellow, N blue, H pink.

C2/*c* space groups. This observation supports our hypothesis of a symmetry breaking and suggests that hydrogen atoms are responsible for it. In fact, since XRD cannot localize them perfectly and in the *Fddd*-type structure they strongly waggle, it is reasonable to expect a lowering of symmetry. Neutron diffraction on $NaND_2$ should be performed to verify our hypothesis.

CONCLUSIONS

In this work, we present a synergic computational and experimental study of $NaNH_2$. All calculations are ab initio and carried out at the athermal limit. In Raman spectra, which are evaluated within the Placzek approximation,[54] room temperature and laser wavelength are approximately taken into account as a simple prefactor to peak intensities. From vibrational calculations, we found its *Fddd* structure to be metastable. A lower-energy structure was identified characterized by C2/*c* symmetry. However, from acquired X-ray diffraction data on single crystals of sodium amide at 80 K, the crystal structure resulted to be still orthorhombic rather than monoclinic. Further analysis should be performed in order to verify if a phase transition occurs at lower temperature. However, analysis of anisotropic displacement parameters of sodium amide atoms in both *Fddd* and C2/*c* space groups supports our hypothesis of a lowering of symmetry because of the very large displacements of H (and D) atoms in the *Fddd*-type structure.

Finally, due to the role of sodium amide in hydrogen storage applications, we also calculated the $NaNH_2$ formation reaction enthalpy from Na and NH_3, which leads to the evolution of H_2. The resulting values at ambient conditions are equal to −12.2 kcal/mol for the orthorhombic system, which is in very good agreement with experimental results (−12.3 kcal/mol).[50]

ASSOCIATED CONTENT

Supporting Information

The Supporting Information is available free of charge at https://pubs.acs.org/doi/10.1021/acs.jpcc.3c02059.

Supplementary material, including (i) additional details on the optimized $NaNH_2$ structures and standardization of monoclinic crystal structure; (ii) analysis of XRD patterns for the monoclinic system, structure factors for both *Fddd*- and C2/*c*-$NaNH_2$ and simulated PXRD pattern considering experimental lattice parameters; and (iii) larger IR and Raman spectra of the two structures (PDF)

AUTHOR INFORMATION

Corresponding Author

Lorenzo Maschio − *Dipartimento di Chimica and NIS centre, Università di Torino, 10125 Torino, Italy;* orcid.org/0000-0002-4657-9439; Email: lorenzo.maschio@unito.it

Authors

Laura Bonometti − *Dipartimento di Chimica, Università di Torino, 10125 Torino, Italy*

Florian Kraus − *Fachbereich Chemie, Philipps-Universität Marburg, 35032 Marburg, Germany;* orcid.org/0000-0003-4368-8418

Tim Graubner − *Fachbereich Chemie, Philipps-Universität Marburg, 35032 Marburg, Germany*

Antti J. Karttunen − *Department of Chemistry, Aalto University, 00076 Aalto, Finland;* orcid.org/0000-0003-4187-5447

Bartolomeo Civalleri − *Dipartimento di Chimica and NIS centre, Università di Torino, 10125 Torino, Italy;* orcid.org/0000-0003-3198-3161

Lorenzo Donà − *Dipartimento di Chimica and NIS centre, Università di Torino, 10125 Torino, Italy;* orcid.org/0000-0001-7735-3881

Complete contact information is available at: https://pubs.acs.org/10.1021/acs.jpcc.3c02059

Notes

The authors declare no competing financial interest.

ACKNOWLEDGMENTS

Funding from the Erasmus+ Cooperation Partnerships programme—VISUENERGY project (2021-1-FI01-KA220-HED-000023408)—is gratefully acknowledged. Authors acknowledge support from the Project CH4.0 under the MUR program "Dipartimenti di Eccellenza 2023-2027" (CUP: D13C22003520001).

REFERENCES

(1) Kraus, C. A. Solutions of Metals in Non-Metallic Solvents; IV.1 Material Effects Accompanying the Passage of an Electrical Current Through Solutions of Metals in Liquid Ammonia. Migration Experiments. *J. Am. Chem. Soc.* **1908**, *30*, 1323−1344.

(2) Kraus, C. A. Reactions and Reagents in Liquid Ammonia. *Chem. Rev.* **1940**, *26*, 95−104.

(3) Birch, A. J.; Macdonald, D. K. C. Metal-Ammonia Solutions. *Nature* **1947**, *159*, 811−812.

(4) Gold, M.; Jolly, W. L.; Pitzer, K. S. A Revised Model for Ammonia Solutions of Alkali Metals. *J. Am. Chem. Soc.* **1962**, *84*, 2264−2265.

(5) Gold, M.; Jolly, W. L. Absorption Spectra of Metal-Ammonia Solutions. *Inorg. Chem.* **1962**, *1*, 818−827.

(6) Warshawsky, I. Stability of a Dilute Solution of Sodium in Liquid Ammonia. *J. Inorg. Nucl. Chem.* **1963**, *25*, 601−605.

(7) Jackman, D. C.; Keenan, C. W. Reactions of Metal-Ammonia Solutions - VI The Alkali Metal-Ammonia Reaction as Catalyzed by Glass. *J. Inorg. Nucl. Chem.* **1968**, *30*, 2047−2057.

(8) Kirschke, E. J.; Jolly, W. L. The Reversibility of the Reaction of Alkali Metals with Liquid Ammonia. *Inorg. Chem.* **1967**, *6*, 855−862.

(9) Watt, G. W.; Barnett, G. D.; Vaska, L. Interaction of Alkali Metals and Liquid Ammonia. *Ind. Eng. Chem.* **1954**, *46*, 1022−1024.

(10) Jepsen, L. H.; Wang, P.; Wu, G.; Xiong, Z.; Besenbacher, F.; Chen, P.; Jensen, T. R. Thermal Decomposition of Sodium Amide, $NaNH_2$, and Sodium Amide Hydroxide Composites, $NaNH_2$−NaOH. *J. Phys. Chem. Chem. Phys.* **2016**, *18*, 25257−25264.
(11) Tarasov, B. P.; Lototskii, M. V.; Yartys', V. A. Problem of Hydrogen Storage and Prospective Uses of Hydrides for Hydrogen Accumulation. *Russ. J. Gen. Chem.* **2007**, *77*, 694−711.
(12) Schlapbach, L.; Zuttel, A. Hydrogen-Storage Materials for Mobile Applications. *Nature* **2001**, *414*, 353−358.
(13) Grochala, W.; Edwards, P. P. Thermal Decomposition of the Non-Interstitial Hydrides for the Storage and Production of Hydrogen. *Chem. Rev.* **2004**, *104*, 1283−1316.
(14) Vajeeston, P.; Ravindran, P.; Kjekshus, A.; Fjellvag, H. Structural Stability of Alkali Boron Tetrahydrides ABH_4 (A = Li, Na, K, Rb, Cs) From First Principle Calculation. *J. Alloys Compd.* **2005**, *387*, 97−104.
(15) Chen, P.; Xiong, Z. T.; Luo, J. Z.; Lin, J. Y.; Tan, K. L. Interaction of Hydrogen with Metal Nitrides and Imides. *Nature* **2002**, *420*, 302−304.
(16) Ichikawa, T.; Hanada, N.; Isobe, S.; Leng, H.; Fujii, H. Mechanism of Novel Reaction from $LiNH_2$ and LiH to Li_2NH and H_2 as a Promising Hydrogen Storage System. *J. Phys. Chem. B* **2004**, *108*, 7887−7982.
(17) Nakamori, Y.; Orimo, S. Destabilization of Li-Based Complex Hydrides. *J. Alloys Compd.* **2004**, *370*, 271−275.
(18) Xiong, Z. T.; Hu, J. J.; Wu, G. T.; Liu, Y. F.; Chen, P. Large Amount of Hydrogen Desorption and Stepwise Phase Transition in the Chemical Reaction of $NaNH_2$ and $LiAlH_4$. *Catal. Today* **2007**, *120*, 287−291.
(19) Ichikawa, T.; Isobe, S. Z. The Structural Properties of Amides and Imides as Hydrogen Storage Materials. *Kristallogr* **2008**, *223*, 660−665.
(20) Sheppard, D. A.; Paskevicius, M.; Buckley, C. E. Hydrogen Desorption from the $NaNH_2$-MgH_2 System. *J. Phys. Chem. C* **2011**, *115*, 8407−8413.
(21) Zhang, Y.; Tian, Q. The Reactions in $LiBH_4$−$NaNH_2$ Hydrogen Storage System. *Int. J. Hydrogen Energy* **2011**, *36*, 9733−9742.
(22) Nagib, M.; Kistrup, H.; Jacobs, H. Neutron Diffraction by Sodiumdeuteroamide, $NaND_2$. *Atomkernenergie* **1975**, *26*, 87−90.
(23) Zhong, Y.; Zhou, H.-Y.; Hu, C.-H.; Wang, D.-H.; Oganov, A. R. Theoretical Studies of High-Pressure Phases, Electronic Structure, and Vibrational Properties of $NaNH_2$. *J. Phys. Chem. C* **2012**, *116*, 8387−8393.
(24) Bai, Y.; Zhao, L.; Wang, Y.; Liu, X.; Wu, F.; Wu, C. Light-Weight $NaNH_2$-$NaBH_4$ Hydrogen Storage Material Synthesized via Liquid Phase Ball Milling. *Int. J. Hydrog. Energy* **2014**, *39*, 13576−13582.
(25) Kaizer, E. B.; Kravchenko, G. N.; Poplavnoi, A. S. A First-Principles Calculations of Electronic Properties of $LiNH_2$ and $NaNH_2$. *J. Struct. Chem.* **2018**, *59*, 1251−1257.
(26) Juza, R.; Weber, H. H.; Opp, K. Kristallstruktur Des Natriumamids. *Z. Anorg. Allg. Chem.* **1956**, *284*, 73−82.
(27) Zalkin, A.; Templeton, D. H. The Crystal Structure of Sodium Amide. *J. Phys. Chem.* **1956**, *60*, 821−823.
(28) Liu, A.; Song, Y. In Situ High-Pressure Study of Sodium Amide by Raman and Infrared Spectroscopies. *J. Phys. Chem. B* **2011**, *115*, 7−13.
(29) Nibler, J. W.; Pimentel, G. C. Infrared Spectrum and Vibrational Potential Function of Amide Ion. *Spectrochim. Acta* **1965**, *21*, 877−882.
(30) Babu, K. R.; Vaitheeswaran, G. Density Functional Study of Electronic Structure, Elastic and Optical Properties of MNH_2 (M = Li, Na, K, Rb). *J. Phys.: Condens. Matter* **2014**, *26*, 235503−235513.
(31) Erba, A.; Desmarais, J. K.; Casassa, S.; Civalleri, B.; Doná, L.; Bush, I. J.; Searle, B.; Maschio, L.; Daga, L. E.; Cossard, A.; et al. CRYSTAL23: A Program for Computational Solid State Physics and Chemistry. *J. Chem. Theory Comput.* **2022**, DOI: 10.1021/acs.jctc.2c00958.
(32) Adamo, C.; Barone, V. Toward Reliable Density Functional Methods without Adjustable Parameters: The PBE0 Model. *J. Chem. Phys.* **1999**, *110*, 6158−6170.
(33) Caldeweyher, E.; Bannwarth, C.; Grimme, S. Extension of the D3 Dispersion Coefficient Model. *J. Chem. Phys.* **2017**, *147*, 034112.
(34) Caldeweyher, E.; Ehlert, S.; Hansen, H.; Neugebauer, S.; Spicher, C.; Bannwarth, C.; Grimme, S. A Generally Applicable Atomic-Charge Dependent London Dispersion Correction. *J. Chem. Phys.* **2019**, *150*, 154122.
(35) Caldeweyher, E.; Mewes, J.; Ehlert, S.; Grimme, S. Extension and Evaluation of the D4 London-dispersion Model for Periodic Systems. *Phys. Chem. Chem. Phys.* **2020**, *22*, 8499−8512.
(36) Oliveira, D. V.; Laun, J.; Peintinger, F. M.; Bredow, T. BSSE-Correction Scheme for Consistent Gaussian Basis Sets of Double- and Triple-Zeta Valence with Polarization Quality for Solid-State Calculations. *J. Comput. Chem.* **2019**, *40*, 2364−2376.
(37) Peintinger, M. F.; Oliveira, D. V.; Bredow, T. Consistent Gaussian Basis Sets of Triple-Zeta Valence with Polarization Quality for Solid-State Calculations. *J. Comput. Chem.* **2013**, *34*, 451−459.
(38) Dovesi, R.; Kirtman, B.; Maschio, L.; Maul, J.; Pascale, F.; Rérat, M. Calculation of the Infrared Intensity of Crystalline Systems. A Comparison of Three Strategies Based on Berry Phase, Wannier Function, and Coupled-Perturbed Kohn-Sham Methods. *J. Phys. Chem. C* **2019**, *123*, 8336−8346.
(39) *STOE WinXPOW V 3.07*; Darmstad, Germany, 2015.
(40) *OPUS V7.2*; Bruker Optik GmbH: Ettlingen, Germany, 2012.
(41) *VistaControl V.4.3.9*; Spectroscopy and Imaging GmbH: Warstein, Germany, 2018.
(42) *X-Area 1.8.1*; STOE & Cie GmbH: Darmstad, Germany, 2018.
(43) Sheldrick, G. M. *SHELXT* - Integrated Space-Group and Crystal-Structure Determination. Acta Cryst. *Acta Crystallogr.* **2015**, *A71*, 3−8.
(44) Sheldrick, G. M. Crystal Structure Refinement With SHELXL. *Acta Crystallogr.* **2015**, *C71*, 3−8.
(45) Hübschle, C. B.; Sheldrick, G. M.; Dittrich, B. J. *ShelXle:* A Qt Graphical User Interface for *SHELXL*. *J. Appl. Crystallogr.* **2011**, *44*, 1281−1284.
(46) D'Amore, M.; Daga, L. E.; Rocca, R.; Sgroi, M. F.; Marana, N. L.; Casassa, S. M.; Maschio, L.; Ferrari, A. M. From Symmetry Breaking in the Bulk to Phase Transitions at the Surface: a Quantum-Mechanical Exploration of Li_6PS_5Cl Argyrodite Superionic Conductor. *Phys. Chem. Chem. Phys.* **2022**, *24*, 22978−22986.
(47) Barrett, C. S. X-Ray Study of the Alkali Metals at Low Temperatures. *Acta Crystallogr.* **1956**, *9*, 671−677.
(48) Voitovich, E. I.; Tolkachev, A. M.; Manzhelii, V. G. Adiabatic Compressibility of Solid Gases. *J. Low Temp. Phys.* **1971**, *5*, 435−446.
(49) Kiefte, H.; Penney, R.; Breckon, S. W.; Clouter, M. J. Brillouin Scattering Studies of Isotopic Effects in Solid Ammonia. *J. Chem. Phys.* **1987**, *86*, 662−665.
(50) Kirschke, E. J.; Jolly, W. L. The Reversibility of the Reaction of Alkali Metals with Liquid Ammonia. *Inorg. Chem.* **1967**, *6*, 855−862.
(51) Coulter, L. V.; Sinclair, J. R.; Cole, A. G.; Roper, G. C. The Heat Capacity, Entropy and Heat Content of Sodium Amide from 15 to 300 °K. The Thermodynamics of Amide Ion in Liquid Ammonia. *J. Am. Chem. Soc.* **1959**, *81*, 2986−2989.
(52) Maschio, L.; Kirtman, B.; Rérat, M.; Orlando, R.; Dovesi, R. Ab Initio Analytical Raman Intensities for Periodic Systems Through a Coupled Perturbed Hartree-Fock/Kohn-Sham Method in an Atomic Orbital Basis. I. Theory. *J. Chem. Phys.* **2013**, *139*, 164101.
(53) Cunningham, P. T.; Maroni, V. A. Laser Raman Spectra of Solid and Molten $NaNH_2$: Evidence for Hindered Rotation of the NH_2^- Ion. *J. Chem. Phys.* **1972**, *57*, 1415−1418.
(54) Maschio, L.; Kirtman, B.; Rérat, M.; Orlando, R.; Dovesi, R. Ab Initio Analytical Raman Intensities for Periodic Systems Through a Coupled Perturbed Hartree-Fock/Kohn-Sham Method in an Atomic Orbital Basis. II. Validation and Comparison with Experiments. *J. Chem. Phys.* **2013**, *139*, 164102.